Maximum Power Point Tracking Injection Method for Islanding Detection of Grid-Connected Photovoltaic Systems in Microgrid

Bakhshi Jafarabadi, Reza; Sadeh, Javad; Popov, Marjan

DOI
10.1109/TPWRD.2020.2976739

Publication date
2020

Document Version
Final published version

Published in
IEEE Transactions on Power Delivery

Maximum Power Point Tracking Injection Method for Islanding Detection of Grid-Connected Photovoltaic Systems in Microgrid

Reza Bakhshi-Jafarabadi, Javad Sadeh, and Marjan Popov, *Senior Member, IEEE*

***Abstract*—This paper proposes a novel islanding detection method (IDM) for grid-connected photovoltaic systems (GCPVSs) through a disturbance injection in the maximum power point tracking (MPPT) algorithm. When an absolute deviation of the output voltage exceeds a threshold, the applied disturbance shifts system operating point from its maximum power point (MPP) condition. This leads to a sharp active power output reduction and consequently, a significant voltage drop in islanded mode beyond the standard voltage limit. The proposed algorithm is defined in a way that the distributed generator (DG) can be restored to MPP after islanding classification. It is thereby effective in microgrid in where the power injection at maximum level to cater the critical loads and maintain the stability of the isolated area are pursued. An intentional time delay has also been considered to avoid nuisance tripping in short-circuit faults which do not require tripping. The assessment of the proposed technique has been conducted for a sample network containing two GCPVSs in a real-time platform including actual relays in hardware-in-the-loop (HiL). The provided results under extensive islanding scenarios defined in islanding standards endorse timely and accurately detection with negligible non-detection zone (NDZ) as well as no false tripping in non-islanding disturbances. The comparative analysis of the presented scheme with a few recent IDMs for GCPVS highlights its overall superiorities, including very small NDZ, fast detection, thresholds self-standing determination, no adverse effect on power quality, and simple and inexpensive integration.**

***Index Terms*—Grid-connected photovoltaic system (GCPVS), Islanding detection method (IDM), Maximum power point tracking (MPPT), Microgrid, Non-detection zone (NDZ).**

I. Introduction

THE penetration of distributed generators (DGs) has significantly risen in the electrical network. Among all DG types, grid-connected photovoltaic system (GCPVS) with the environmental, technical, and economic benefits is proven to be the most promising technology during the past decade [1]. The connection of this resource, however, poses a few protection and safety issues in distribution network such as islanding [2]. Islanding refers to a condition where energized DGs, supplying solely the local loads, are disconnected from the bulk power system. This operation mode is harmful to the maintenance crew who supposed a de-energized line. The customer equipment can also be damaged by out-of-phase reclosing transients. IEEE 1547-2008 and UL 1741 standards postulate 2 seconds as the maximum time to cease energizing DG after islanding inception [3], [4]. However, a fast detection and trip before auto-reclosing to avoid large voltage transient is required. The fast detecting of islanding operation is a mandatory feature for DGs of microgrid for seamless reconnection to maintain the system stability and feeding critical loads as well [5].

Islanding detection methods (IDMs) are broadly categorized to remote and local groups. Communication capabilities which are grown over the past decades, provide possibilities for examining the connection of DGs to the network in remote IDMs [6], [7]. When the connection of the signal generator and receiver embedded in the upstream substation and DG(s) location is failed, islanding is reported. Although these schemes are fast and reliable, they are not economically viable especially for small scale DGs.

In local methods, a feature of point of common coupling (PCC), i.e., the point that DG(s) and local load(s) are connected to the network, is continuously monitored. These techniques are divided into passive, active, and hybrid subgroups. Loss of main (LOM) has been identified in passive IDMs when a local yardstick deviates its tolerable range regarding the cut of active and reactive powers received from or injected into the grid. Under/over frequency (UF/OF) [8], under/over voltage (UV/OV) [9], rate of change of frequency (ROCOF) [10], rate of change of equivalent resistance to the angular velocity [11], rate of change of reactive power [12], aggregate voltage variation index [13], and DC voltage ripple [14] are some examples among the recent passive IDMs. Despite the simple and cost-effective implementation, these methods suffer a large non-detection zone (NDZ), i.e., the cases that IDM fails to detect islanding. Pattern recognition techniques [15], [16] and frequency-based transformations [17]–[20] are newly developed for islanding detection. These mathematical tools are proved to be accurate classifiers; however, the high dependency on the case study system and large time for processing big data have been reported as their main demerits.

Manuscript received September 24, 2019; revised December 27, 2019; accepted February 21, 2020. Date of publication February 27, 2020; date of current version January 22, 2021. Paper no. TPWRD-01083-2019. *(Corresponding author: Javad Sadeh.)*

Reza Bakhshi-Jafarabadi and Javad Sadeh are with the Department of Electrical Engineering, Ferdowsi University of Mashhad, Mashhad +918, Iran (e-mail: r.bakhshi@mail.um.ac.ir; sadeh@um.ac.ir).

Marjan Popov is with the Delft University of Technology, 2628CD Delft, The Netherlands (e-mail: m.popov@tudelft.nl).

Color versions of one or more of the figures in this article are available online at http://ieeexplore.ieee.org.

Digital Object Identifier 10.1109/TPWRD.2020.2976739

Active IDMs such as impedance measurement [21], active ROCOF [22], voltage positive feedback (VPF) [23], [24] and its improvement [25], [26], and *d*–axis equivalent resistance [27] have been mostly introduced for inverter-based DGs to mitigate the NDZ. To this end, an intentional disturbance has been injected in a way that a local variable has been unstabilized in islanding mode. Although these techniques have advanced smaller NDZ, the applied disturbance deteriorates the power quality of the distribution network. Finally, a combination of the active and passive IDMs to achieve smaller NDZ and lower power quality degradation known as hybrid methods have been recommended [28], [29]. The active disturbance is actuated while the passive technique detects suspicious islanding condition. Hence, the power quality has not been affected in normal operating points.

This paper deals with a novel methodology for detecting the islanding operation of GCPVS. When an absolute deviation of the output voltage surpasses a threshold, a disturbance is injected into the maximum power point tracking (MPPT) algorithm. This disturbance shifts GCPVS operating point from its maximum power point (MPP) condition, resulting in a significant active power output reduction. Consequently, it drops sharply the output voltage in islanded mode beyond the standard limit. On contrary, this active power output fall has a negligible effect on DG's terminal voltage when it operates in parallel with the utility. The advantages of the proposed IDM can be listed as follows:

- Accurate classification with near zero NDZ.
- Fast detection within 300 ms.
- Quick power restoration to MPP, making it convenient for seamless reconnection purpose in microgrids.
- Self-standing determination of the thresholds regardless of the system parameters.
- Straightforward and inexpensive implementation to the existing voltage source inverters (VSIs).
- No negative effect on the power quality of the network.

The rest of the paper is structured as follows; the proposed algorithm is described in Section II. The introduction of the case study system containing two power plant GCPVSs and evaluation of the provided scheme under extensive islanding and non-islanding scenarios are presented in Section III. Section IV elaborates the selection criteria of the thresholds in the term of NDZ. Section V presents method discussion, including the effect of presented strategy on protection of the radial distribution network and a comparison between the current algorithm and a few IDMs developed for GCPVSs. Finally, concluding remarks are discussed in Section VI.

II. Description of the Proposed Method

According to Fig. 1, the grid-tie VSI consists of two independent controllers; current control loop that balances the input and output powers and controls the power quality of the output current, and voltage control loop which is responsible for MPPT [30]. The MPPT is accomplished through perturbing a disturbance in PV module's voltage and observing the result on the DC link power (P_{DC}). The same disturbance is injected in

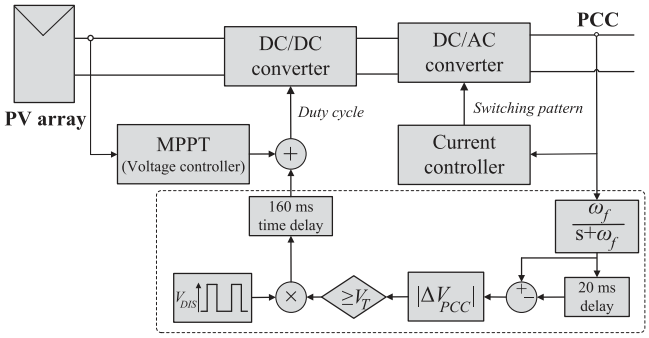

Fig. 1. Implementation of the proposed algorithm in VSI.

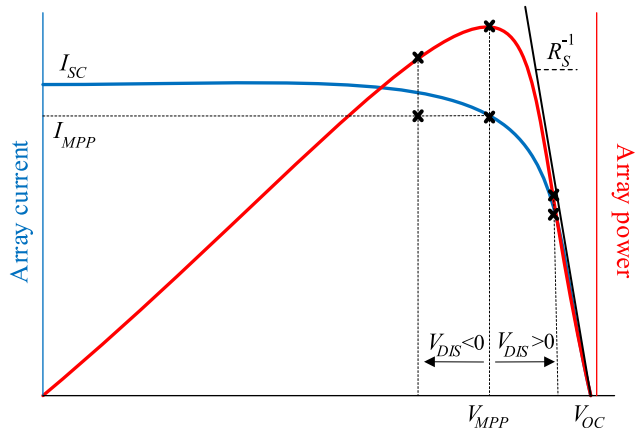

Fig. 2. MPPT and proposed IDM realizations in PV array characteristics.

the positive power variation while its direction is toggled in the power drop instance. The reference voltage corresponds to MPP is then used to set the duty cycle of the DC/DC converter [31].

In the proposed IDM, a disturbance is inserted into the MPP reference voltage of the MPPT algorithm (V_{MPPref}) as shown by dash line in Fig. 1:

$$V_{MPPref} = V_{MPP} + V_{DIS} \tag{1}$$

where V_{DIS} and V_{MPP} are disturbance voltage and MPP voltage determined by MPPT algorithm, respectively. Based on power over voltage characteristics of the PV array illustrated in Fig. 2, this disturbance voltage can be added or subtracted for MPP lost purpose. However, the power fall for the positive disturbance (in the right-hand side of MPP) is much sharper. A greater power drop is therefore achieved for positive injection with a same disturbance level. It worth to mention that V_{OC}, I_{SC}, and I_{MPP} in Fig. 2 are open-circuit voltage, short-circuit current, and MPP current, respectively.

As provided in the flowchart of the proposed algorithm in Fig. 3, this disturbance is activated when the absolute deviation of the PCC voltage $(|\Delta V_{PCC}|)$ in any phase exceeds a voltage threshold (V_T). The MPP deviation leads to a notable active power output drop. In the normal operation mode, this power fall has small effect on the output voltage due to the network presence. On the other hand, it reduces the PCC voltage (V_{PCC})

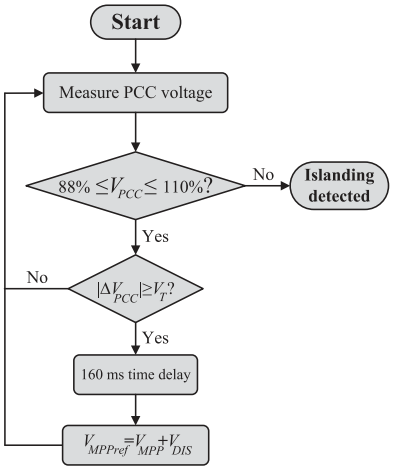

Fig. 3. Flowchart diagram of the suggested algorithm.

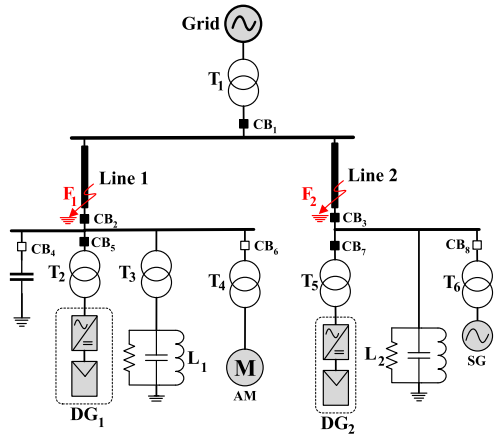

Fig. 4. An illustration of the case study system.

in islanded mode regarding the following equation:

$$P_{DG} = \frac{V_{PCC}^2}{R} \tag{2}$$

where P_{DG} represents the DG's active power output and *R* is the resistive part of the parallel RLC local load modeled in IEEE 929 [32]. This significant voltage collapse passes minimum tolerable voltage edge (88%) [3], [4] and LOM is identified.

The voltage is again restored to MPP level after a transient through the MPPT algorithm. Therefore, while this voltage drop can be used to recognize the islanding incident, the DG can continue power generation at MPP mode in the microgrid regarding the fast restoration of the reference voltage to MPP. This is an advantage of the proposed IDM, making it applicable to microgrids in where catering the critical loads and preserving voltage and frequency stabilities are mandatory. In addition, the suggested disturbance declines P_{DG} based upon the above explanation, i.e., the amplitude of the output voltage and current for a given linear load. Hence, the harmonic distortion produced is unnoticeable and its adverse effect on the output power quality does not represent a major issue.

III. Evaluation of the Proposed Algorithm

The assessment of the proposed scheme has been carried out through several hardware-in-the-loop (HiL) real-time simulations in RSCAD environment. Fig. 4 and Table I provide the prototype system, including two parallel feeders, each containing a DG and local load in where L_1 and L_2 represent household and commercial consumers, respectively. The DGs equipped with the proposed IDM are constructed in software using four RTDS PB5 cards. Two commercial multi-function relays (CB_5 and CB_7 in Fig. 4) with settings matched with IEEE 1547-2008 [3] are connected in HiL.

A 20% disturbance is injected in V_{MPPref} if $|\Delta V_{PCC}|$ surpasses 0.4% in any phase, i.e., V_T and V_{DIS} are supposed to 0.4% and $0.2V_{MPP}$; however, a comprehensive explanation of settings selection is presented in Section IV. This disturbance has been injected for 300 ms time interval and has been turned off after that for a 1.7 s time frame, i.e., the total period is 2 s. In addition, it is intentionally inserted after a 160 ms time delay to avoid mal-operation of the relay installed at the DG end under transient faults which do not require tripping, i.e., $V_{PCC} < 50\%$ lasts for a duration shorter than 160 ms. This time corresponds to the time delay of the UV protection in compliance with IEEE 1547-2008 [3].

TABLE I
Case Study System Settings

Equipment	Description
Grid	400 kV, 1000 MVA, 50 Hz
Line	Line 1: 5 km, Z^+=0.17+j1.56 (Ω), Z^0=1.16+j4.55 (Ω) Line 2: 15 km, Z^+=0.44+j4.63 (Ω), Z^0=3.49+j13.65 (Ω)
Transformer	T_1: 4.8 MVA, 400/13.2 kV, ΔY11 T_2, T_3: 1.2 MVA, 13.2/0.4 kV, ΔY11 T_4: 1 MVA, 13.2/0.4 kV, ΔY11 T_5: 3.6 MVA, 13.2/0.4 kV, ΔY11 T_6: 8 MVA, 13.2/20 kV, ΔY11
GCPVS*	DG_1: 1 MW at STC, DG_2: 3 MW at STC PV module (YL305P-35b): V_{OC}=46.3 V, I_{SC}=8.87 A, V_{MPP}=37.0 V, I_{MPP}=8.25 A
SG	2–8 MW, 20 kV, 50 Hz, four poles, Inertia constant: 1.1 s
AM	250–1000 HP, 0.4 kV, R_s=0.0425 pu, L_s=0.087 pu, R_r=0.05 pu, L_r=0.0658 pu, L_m=2.9745 pu

*The GCPVSs work at unity power factor ($Q_{DG} = 0$ Mvar).

In GCPVSs, the aggregate PV module has been modeled in the real-time platform itself based on the well-defined single-diode model [33]. The VSI's voltage and current control loops incorporate perturb and observe (P&O) and pulse width modulation (PWM) algorithms with 0.1 kHz and 2 kHz frequencies, respectively [30]. Asynchronous motor (AM) and capacitor bank are also connected to the weakest feeder for simulating the non-islanding events while a synchronous generator (SG) is connected to the second feeder to simulate hybrid DGs scenario.

Analog and digital inputs/outputs are then sent to a pair of actual multi-functional digital relays. The interface of the relays and PCCs' quantities are realized through two amplifiers and a gigabit transceiver analogue card (GTAO). The output of the proposed IDM is sent to these relays to disconnect DG(s) in

TABLE II
RESULTS FOR VARIOUS ISLANDING SCENARIOS IN SINGLE DG CONNECTION

Case no.	Event description	Load 1 at 0.4 kV LL				$P_L^1 + j\,Q_L^1$	ΔP	ΔQ	**Detection Time**
		R_1 (mΩ)	L_1 (mH)	C_1 (mF)	Quality factor	(MW/Mvar)	(%)	(%)	**(ms)**
1	Active power mismatches (at STC)	188.23	–	–	–	0.85 + j 0.00	+15	0	**275**
2		177.77	–	–	–	0.90 + j 0.00	+10	0	**272**
3		168.42	–	–	–	0.95 + j 0.00	+5	0	**274**
4		160	–	–	–	1.00 + j 0.00	0	0	**–**
5		152.38	–	–	–	1.05 + j 0.00	-5	0	**191**
6		145.45	–	–	–	1.10 + j 0.00	-10	0	**190**
7		139.13	–	–	–	1.15 + j 0.00	-15	0	**185**
8	Active/reactive power mismatches (at STC)	162	–	0.9952	–	0.99 - j 0.05	+1	+5	**205**
9		162	10.19	–	–	0.99 + j 0.05	+1	-5	**216**
10		158	–	0.9952	–	1.01 + j 0.05	-1	+5	**210**
11		158	10.19	–	–	1.01 - j 0.05	-1	-5	**207**
12		168.42	–	0.9952	–	0.95 - j 0.05	+5	+5	**197**
13		168.42	10.19	–	–	0.95 + j 0.05	+5	-5	**202**
14		152.38	–	0.9952	–	1.05 - j 0.00	-5	+5	**200**
15		152.38	10.19	–	–	1.05 + j 0.05	-5	-5	**196**
16	Active/reactive power mismatches (at 500 W/m^2 and 25 °C)	323.23	–	0.0995	–	0.495 - j 0.005	+1	+1	**240**
17		323.23	101.9	–	–	0.495 + j 0.005	+1	-1	**249**
18		316.83	–	0.0995	–	0.505 - j 0.005	-1	+1	**257**
19		316.83	101.9	–	–	0.505 + j 0.005	-1	-1	**219**
20		323.23	–	0.4976	–	0.495 - j 0.025	+1	+5	**204**
21		323.23	20.38	–	–	0.495 + j 0.025	+1	-5	**222**
22		316.83	–	0.4976	–	0.505 - j 0.000	-1	+5	**227**
23		316.83	20.38	–	–	0.505 + j 0.025	-1	-5	**231**
24	Load quality factors (at STC)	158	1.019	9.952	0.5	1.01 + j 0.00	-1	0	**218**
25		158	0.509	19.904	1.0	1.01 + j 0.00	-1	0	**222**
26		158	0.339	29.856	1.5	1.01 + j 0.00	-1	0	**317**
27		158	0.254	39.809	2.0	1.01 + j 0.00	-1	0	**286**
28		158	0.204	49.761	2.5	1.01 + j 0.00	-1	0	**297**
29	Unbalanced load (at STC)	160/160/130	–	–	–	1.05 + j 0.00	-5	0	**190**
30		160/160/190	–	–	–	1.00 + j 0.00	0	0	**267**
31		130/160/190	–	–	–	0.95 + j 0.00	+5	0	**202**

The index "1" implies the first load and DG characteristics.

TABLE III
PERFORMANCE OF THE PROPOSED TECHNIQUE UNDER ZIP LOADS

Case no.	$P_L^{nom} + j\,Q_L^{nom}$	α_p	**Detection Time (ms)**
32	2.97 MW + j 0.00 Mvar	0.00	**189**
33		0.25	**176**
34		0.50	**214**
35		0.75	**213**
36		1.00	**222**
37		1.25	**224**
38		1.50	**227**
39		1.75	**232**
40		2.00	**259**

TABLE IV
CASE STUDIES AND OUTPUTS OF THE MULTI DGS STUDY

Case no.	$P_L^T + j\,Q_L^T$ (MW/Mvar)	ΔP (%)	ΔQ (%)	**Detection Time (ms)**
41	3.96 - j 0.20	+1	+5	**206**
42	3.96 + j 0.00	+1	0	**192**
43	3.96 + j 0.20	+1	-5	**191**
44	4.04 - j 0.20	-1	+5	**192**
45	4.04 + j 0.00	-1	0	**196**
46	4.04 + j 0.20	-1	-5	**180**

TABLE V
RESULTS OF HYBRID DGS SCENARIO UNDER A SET OF ΔP

Case no.	P_{SG} (MW)	P_{DG2} (MW)	P_{L2} (MW)	ΔP (%)	**Detection Time (ms)**
47	1.00	3.00	3.96	+1	**507**
48	1.00		4.04	-1	**259**
49	1.00		4.20	+5	**216**
50	1.00		3.80	-5	**240**
51	2.00		4.75	+5	**317**
52	4.00		6.65	+5	**413**
53	6.00		8.55	+5	**–**

conventional power system or change settings for standalone operation of microgrid.

A. Islanding Conditions

This part explores the authenticity of the proposed technique under several islanding scenarios detailed in Tables II–V. The

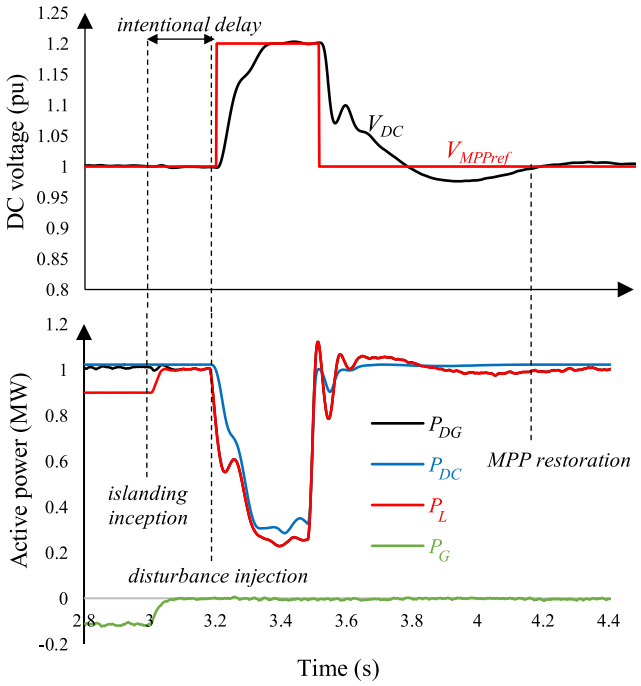

Fig. 5. Results for 10% surplus active power in islanded area.

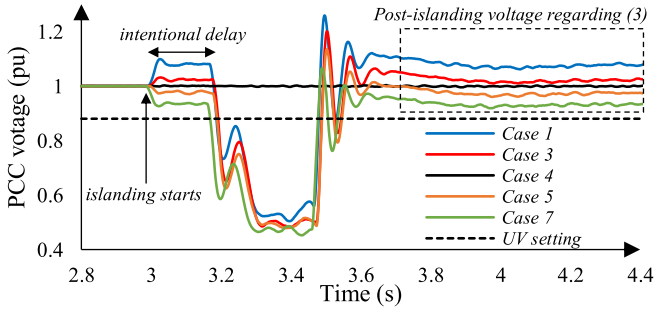

Fig. 6. PCC voltage under various loading levels.

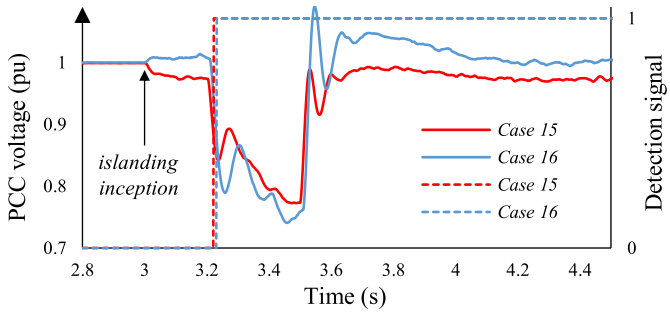

Fig. 7. Outputs under reactive power mismatch and non-full rated generation.

real-time simulations for islanding events, yielded at $t = 3$ s, have been presented and thoroughly analyzed.

1) Active/Reactive Power Mismatches (Cases 1–23): When the grid is lost, the voltage and frequency of the isolated region deviate from its pre-islanding settings owing to the active (ΔP) and reactive power mismatches (ΔQ). It is observed that regarding the amount of active power imbalance, the voltage has been changed to the new level after separation as in (3):

$$\Delta P = P_{DG}\left(1 - \frac{V_{pr}^2}{V_{po}^2}\right) \tag{3}$$

where V_{pr} and V_{po} are the pre- and post-islanding voltages [9]. While the relative active power mismatch $(\Delta P/P_{DG})$ lies inside the -29.13 to 17.35% range, V_{po} would not leave the standard range for $V_{pr} = 100\%$. Therefore, LOM has not been found by traditional voltage relays in such situations.

The initial simulations have been conducted to this end for purely resistive load with real power imbalances inside the relay's NDZ (cases 1–7) at standard test condition (STC), i.e., the situation that cell temperature and received radiation are 25 °C and 1000 W/m^2. The results, including the PV voltage, MPP reference voltage, and active powers (for case 2) as well as DG's terminal voltage have been depicted in Figs. 5 and 6, respectively in where P_L and P_G are load and grid active powers.

It is readily observed that the presented IDM lessens successfully the active power output for drifting voltage beyond the UV relay setting except in zero mismatch case (scenario 4). Because the voltage change for $\Delta P = 0\%$ is zero after isolation, the provided disturbance has not been triggered and LOM remains undetected. Hence, the proposed scheme fails to classify islanding for $|\Delta V_{PCC}| < V_T$, e.g., the NDZ includes $-0.805\% < \Delta P/P_{DG} < 0.795\%$ for $V_T = 0.4\%$. The detailed relation between V_T and NDZ will be outlined in the next section.

The MPP is regained within 1–1.2 s providing the chance of power generation at maximum level in the autonomous mode. In Fig. 6, the post-islanding voltage after disturbance clearance can be defined by (3) as well.

IEEE 1547-2008 and UL 1741 standards emphasize on anti-islanding tests in non-full rated DG penetration as well as small active/reactive power mismatches up to ±5%. The HiL real-time simulations have been accordingly developed for various active and reactive power imbalances at STC (cases 8–15) and 500 W/m^2 received irradiance (cases 16–23). The method's detection signal and PCC voltage graphs of cases 15 and 16 have been rendered in Fig. 7. It can be inferred from Table II and PCC voltage waveforms that the MPPT-based injection technique is highly reliable under aforementioned scenarios. Moreover, the classification time for various case studies is within 280 ms, meeting the islanding detection standards and small enough for quick reconnection in microgrid.

2) Load Quality Factor (Cases 24–28): Load quality factor (Q_f) has been reported as a critical variable in active IDMs performance. IEEE 1547-2008 and UL 1741 postulate the detecting of islanding operation under quality factors lower than 1 and 2.5 within 2 seconds, respectively [3], [4]. Therefore, scenarios 24–28, with quality factors in the 0.5–2.5 range, 50 Hz resonant frequency and negligible active power mismatch, are simulated and the DG's voltage is shown in Fig. 8. The outputs zoomed for 2.8–4.2 s time framework clearly reveal an accurate voltage decline and islanding detection in all cases. Since the power generation in the isolated

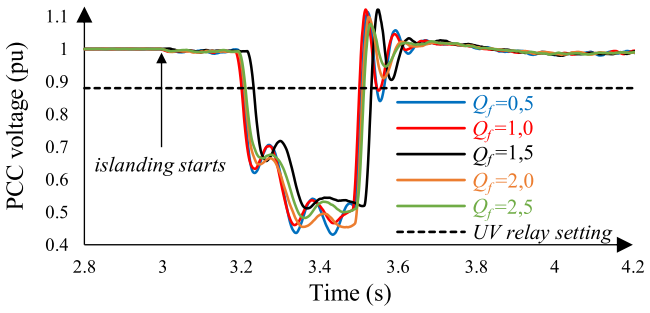

Fig. 8. Performance of the proposed algorithm under several Q_f levels.

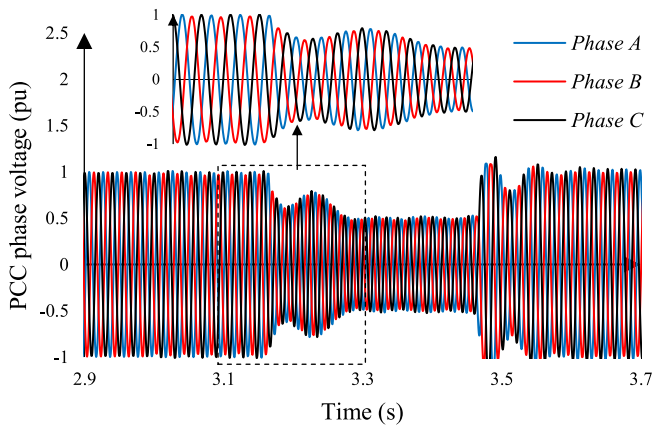

Fig. 9. Voltage phases during islanding phenomenon of unbalanced loading.

area is close to the load consumption, the PCC voltage is re-established around the nominal level after 1 s (MPP achievement) and hence the islanding to autonomous transition is fully facilitated.

3) Unbalanced Loading (Cases 29–31): The balanced loading is rarely occurred in real three-phase network. This condition can mislead the method's performance or increase the detection time, e.g., from 0.2 s to 1.1 s in [19]. The analysis of such cases is hence crucial. Since the proposed method exploits the voltage measurement and comparison of every phase with threshold for disturbance activation, it is able to find islanding under unbalanced loading too. This capability has been demonstrated in cases 29–31 for purely resistive load. The respective resistances in phases A, B, and C in Table II are designed for simulating $+5\%$, -5% and zero three-phase power mismatches. What stands from the phase voltage in Fig. 9 (for case 31), the method is precisely shifted all phases to the lower edge and identified LOM. Therefore, its performance in unbalanced loading states is highly secure.

4) Static Load (Cases 32–40): IEEE 929 recommends local load modeling as a constant parallel RLC branch [32]. However, most loads represent voltage-based and/or frequency-dependent behavior in practical applications. Since the current technique diminishes P_{DG} and V_{PCC} during islanding phenomenon, its performance at the presence of such loads, especially constant power, would be interesting. In this study, the second load (L_2) has been substituted by a static load with the following

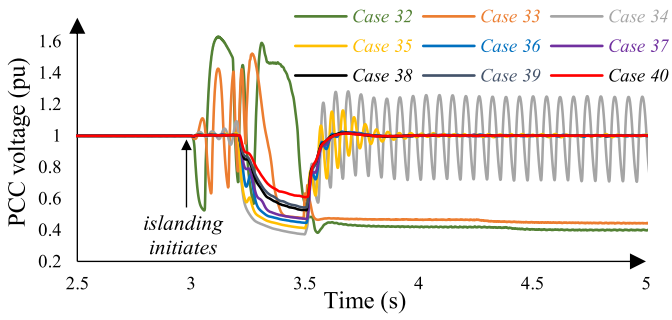

Fig. 10. Results of ZIP load tests.

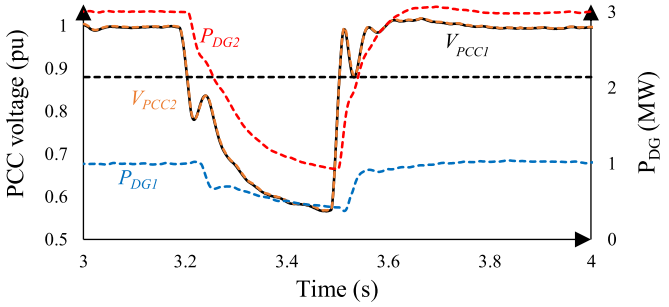

Fig. 11. Outputs in multi DGs islanding phenomenon (case 44).

characteristics, focusing on PCC voltage dependency:

$$\begin{cases} P_L^{new} = P_L^{nom} \times \left(\frac{V_{PCC}^{new}}{V_{PCC}^{nom}}\right)^{\alpha_p} \\ Q_L^{new} = Q_L^{nom} \times \left(\frac{V_{PCC}^{new}}{V_{PCC}^{nom}}\right)^{\alpha_q} \end{cases} \tag{4}$$

where nominal and new arbitrary conditions have been denoted by "*nom*" and "*new*", respectively. Moreover, α_p and α_q are the model coefficients, e.g., 0, 1, and 2 represent constant power (P), current (I), and impedance loads (Z), respectively [24]. Cases 32–40 in Table III show the results related to islanding under ZIP loads with several α_ps and $+1\%$ active power mismatch.

It is inferred from Fig. 10 that the PCC voltage has been unstabilized after island formation for the scenarios 32–34 with a very small α_p (constant power load) to satisfy $P_{DG} = P_L$ before disturbance insertion. In other situations, in which the voltage remains within standard ranges, the power drop caused by the proposed scheme boosts voltage instability/variation and pushes it out of tolerable range. Consequently, the presented algorithm is an effective islanding classifier for all load types.

5) Multi DGs Connection (Cases 41–46): It has been stated in the literature that some active techniques suffered controllers' interference and misclassification in the multi DGs scenario [21]. The tests have been hence extended for two power plant GCPVSs through opening CB_1 in Fig. 4 with total generation of 4 MW closely matched to the loads demand (P_L^T and Q_L^T). The studies correspond to this part are listed in Table IV and a sample outcome in case 44 is given in Fig. 11. According to the output power and voltage graphs, the MPP is lost intentionally for a short duration so that the DG's terminal voltage crosses the minimum permissible voltage. DC voltage is also reinstated to

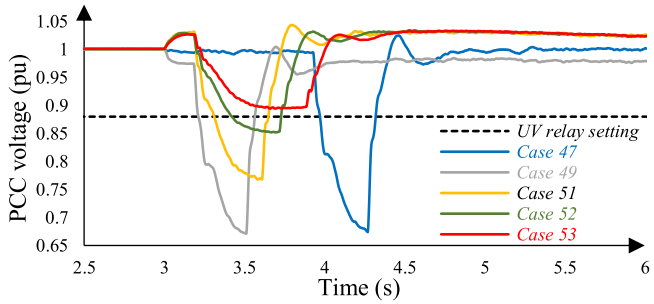

Fig. 12. Analysis and outputs of the hybrid DGs case studies.

MPP after disturbance clearance for probable utilization in the autonomous mode.

6) Hybrid Distributed Generation (Cases 47–53): The next analysis is related to a hybrid DGs condition. A synchronous generator (SG) is connected through CB_8 and the second load is adjusted for scenarios 47–50 to simulate a few active power imbalances (Table V). In this table, P_{SG}, P_{DG2}, and P_{L2} are the active powers of SG, second GCPVS, and the second load, respectively. Fig. 12 displays the PCC voltage of a few case studies measured at the second GCPVS terminal.

After islanding onset, the injected disturbance declines P_{DG2} by 76% under $V_{DIS} = 0.2V_{MPP}$. This power reduction drops the PCC voltage until passing the UV protection setting. It is seen in Table V that the detection time is elevated in some cases regarding the higher equivalent system inertia in comparison to the purely inverter interfaced DGs, e.g., GCPVSs.

Since GCPVSs contribute only to active power reduction and the response speed of the total DG units at the presence of SG is diminished, a further analysis is mandatory. In this perspective, (3) is modified as in (5):

$$\Delta P_{DIS} = P_{DG}^{T}\left(1 - \frac{V_{pr}^2}{V_{po}^2}\right) \tag{5}$$

where P_{DG}^{T} and ΔP_{DIS} are total active power generation of all DGs and the active power drop of GCPVSs created by the proposed disturbance. The power reduction of the second GCPVS is 2.28 MW for $V_{DIS} = 0.2V_{MPP}$. Referring to (5), V_{po} would thereby cross 88% under $V_{pr} = 100\%$ whilst the DGs' active power production would be smaller than 7.83 MW. Otherwise, the power reduction created by the presented disturbance cannot push voltage beyond the UV relay setting. The output voltage response to the injected disturbance might be also slow so that it does not settle at its steady-state condition, which is designed to be under 88%.

The performance of the suggested algorithm under such situations can be improved by raising the disturbance size or/and increasing the duration time of the applied disturbance. In the first approach, the disturbance is strong enough to shift the voltage beyond 88% even when it does not reach to the new steady-state operating point. In the latter strategy, the disturbance lasts for a longer time, e.g., 600 ms; accordingly, the voltage has enough time to settle at the new steady-state situation, which is beyond 88%.

TABLE VI
NON-ISLANDING DISTURBANCES SCENARIOS

Case no.	Description	Power change	Method activated?/Detection?
1	Capacitor bank connection (closing CB_4)	0.25 Mvar	Yes/No
2		0.50 Mvar	Yes/No
3		0.75 Mvar	Yes/No
4		1.00 Mvar	Yes/No
5	Asynchronous motor starting (closing CB_6)	250 HP	Yes/No
6		500 HP	Yes/No
7		750 HP	Yes/No
8		1000 HP	Yes/No
9	Sudden L_1 rise (Normally 1 MW)	3 MW	Yes/No
10		3 MW, +3 Mvar	Yes/No
11		3 MW, -3 Mvar	Yes/No

TABLE VII
RESULTS FOR TRANSIENT SHORT-CIRCUIT FAULTS

Case no.	Fault description	R_F (Ω)	Time with V_{PCC}<50% (ms)*	
			F_1	F_2
10	AG with *FCT*=100 ms	0.01	89.1	99.1
11		1	81.3	118.3
12		5	0	11.5
13		20	0	0
14	ABG with *FCT*=120 ms	0.01	119.5	110.9
15		1	118.1	114.2
16		5	118.0	0
17		20	117.1	0
18	AB with *FCT*=150 ms	0.01	0	55.3
19		1	0	0
20	ABCG with *FCT*=159 ms	0.01	151.9	158.1
21		1	153.9	154.8
22		5	0	0
23		20	0	0

**VPCC* represents for PCC voltage of the faulted phase(s).

The analysis has been developed in cases 51–53 for a set of SG penetration levels while the disturbance is triggered for 600 ms. The results in Fig. 12 indicate successful islanding classification of the proposed IDM in hybrid DGs case except in scenario 53 that the total generation is 9 MW. In this situation, the PCC voltage reduces to 90.3% and islanding remains undetected.

B. Non-Islanding Conditions (Cases 1–23)

There are several incidents which probably fluctuate the PCC voltage and trigger the embedded disturbance. Although the activation of the proposed algorithm and active power output reduction for a short duration are inevitable, it should not descend the PCC voltage to the lower standard margin. The transient caused by this disturbance has to be settled down in a limited time interval as well. Some non-islanding switching events detailed in Table VI have been examined in this regard at the weakest feeder (near to the first DG). These scenarios include capacitor switching, abrupt load change, and motor starting.

Moreover, various types of short-circuit faults with different fault resistance (R_F) and fault clearance time (*FCT*) have been taken into account in Table VII. The short-circuit tests have been arranged at the end of two lines (F_1 and F_2 in Fig. 4) in a way that the relays equipped at the DGs' end do not trip them in accordance with IEEE 1547-2008 [3]. In order to evade false tripping in such cases, the proposed disturbance has been

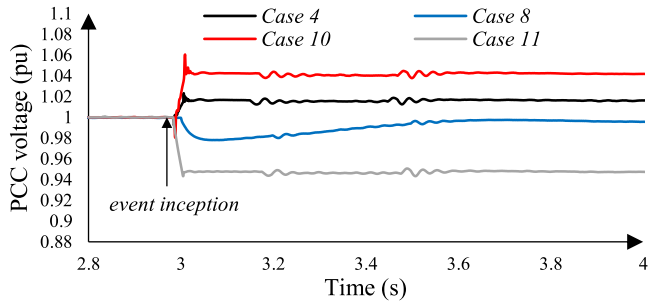

Fig. 13. Outputs of the proposed IDM under non-islanding events.

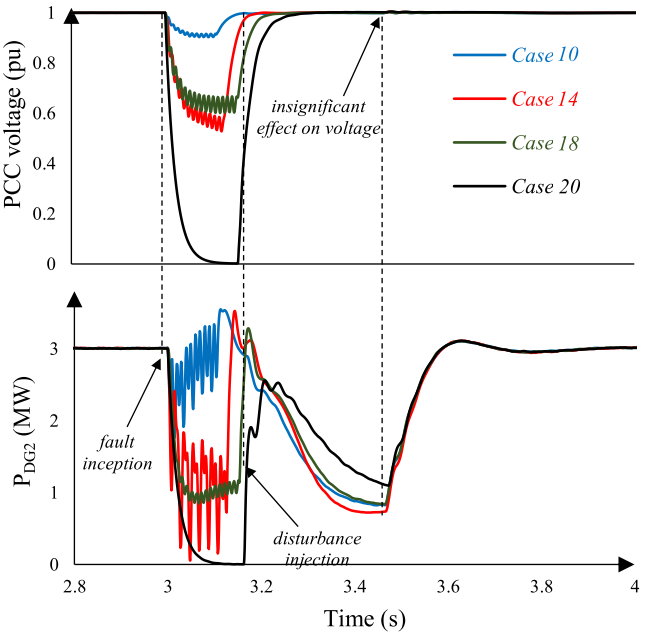

Fig. 14. Results of short-circuit faults at the end line of second feeder (F_2).

intentionally integrated with 160 ms time delay as explained earlier. Therefore, although the disturbance diminishes the DG's generation after fault clearance, the voltage has not been notably influenced by it since the fault is removed.

The first DG's terminal voltage in Fig. 13 for non-islanding events does not depart the 88–110% range and the DG returns to MPP in all cases. The outcomes in Table VII highlight that the proposed disturbance does not affect the time duration of the PV units' voltage collapse during the faults, and the relays do not classify wrongly such events as islanding (Fig. 14). Therefore, the proposed IDM exhibits no false tripping in the switching transients and provides the chance of UV-ride through under short-circuit faults which do not require tripping.

IV. Selection of the Threshold Settings

In the recommended scheme, the disturbance has been triggered when the absolute deviation of PCC voltage exceeds a voltage threshold (V_T). The amplitude of the applied disturbance (V_{DIS}) is another setting should be precisely selected to

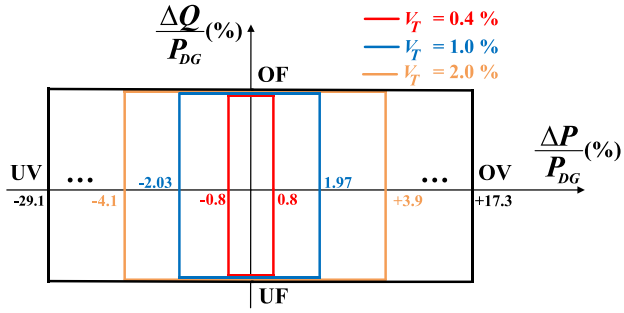

Fig. 15. Effect of voltage threshold on NDZ.

adequately deviate DG from MPP for $V_{PCC} < 88\%$ purpose. The selection criteria of these settings are elaborated as follows.

A. Voltage Threshold (V_T) for Disturbance Activation

In the current methodology, lower selection of V_T leads to smaller NDZ. The rate of nuisance activation upon PCC voltage fluctuations of the grid-connected switching incidents can be risen as well. Since the duration of the MPP loss is too short, the voltage threshold selection is done in the term of NDZ.

The NDZ can be measured by employing (3) for various V_T under $V_{pr} = 100\%$. For a given V_T, NDZ includes the relative active power mismatches that result in V_{po} with $|V_{po} - V_{pr}| < V_T$. This procedure has been performed under a few V_T and the results have been illustrated in Fig. 15. The computed NDZ in the relative active and reactive power mismatches ($\Delta P/P_{DG}$ and $\Delta Q/P_{DG}$) plate highlights small blind zone of the proposed IDM against standard voltage relays and available methods.

B. MPP Disturbance Voltage (V_{DIS})

The proposed method tries to push PCC voltage to the lower limit under islanding events. Accordingly, the MPP deviation should be large enough to provide this PCC voltage drift. The maximum output voltage shift occurs at the transition from the upper allowable edge (110%) to the lower one (88%). Equation (3) indicates that the minimum required active power fall under this transition ($V_{pr} = 110\%$ and $V_{po} = 88\%$) is -56.25% regardless of the system features and DG penetration level.

The slope of PV array's power vs. voltage graph in the right-hand side of MPP is used to figure out the required disturbance voltage. This slope can be estimated by a series resistance, defined in the single-diode representation of the PV array (R_S in Fig. 2) [33]. By considering the voltage and current of the new operating point after disturbance injection as V_{new} and I_{new}, the following equation can be derived:

$$R_S^{-1} = \frac{I_{new}}{V_{new} - V_{OC}} = \frac{I_{MPP}}{V_{MPP} - V_{OC}} \tag{6}$$

By assuming $V_{OC} = (1+\beta)V_{MPP}$ and $V_{new} = (1+\alpha)V_{MPP}$ and manipulating (6), the new current can be expressed

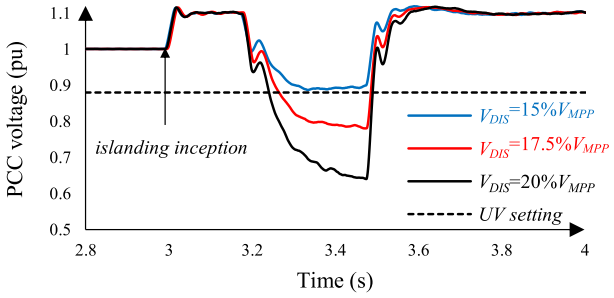

Fig. 16. Disturbance size impact on effective detection.

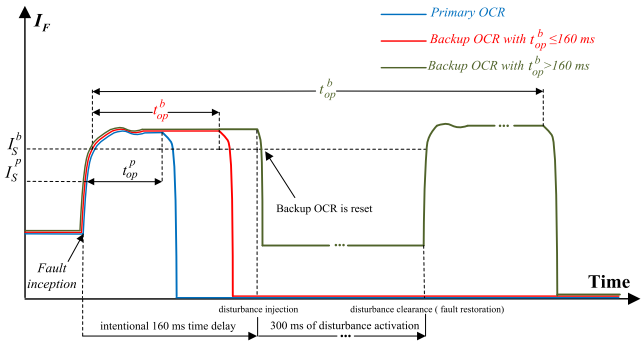

Fig. 17. Effect of proposed algorithm on instantaneous and DT OCRs.

as:

$$I_{new} = I_{MPP}(\beta - \alpha)\beta^{-1} = I_{MPP}(1 - \alpha\beta^{-1}) \quad (7)$$

where β can be determined through the ratio of V_{OC} to V_{MPP} in STC and can be found in the PV module datasheet. This parameter is conventionally within the 20–30% range, e.g., 25% for YL305P-35b (Table II). α is also the unknown variable which should be determined for disturbance selection, i.e., $V_{DIS} = \alpha V_{MPP}$. This parameter should be limited to β to obtain stable performance of DC/DC converter ($V_{new} \leq V_{OC}$) as well. The both sides of (7) can be multiplied by V_{new} to reach the new DC link power (P_{new}) expression after disturbance activation:

$$P_{new} = V_{new} \times I_{new} = P_{MPP}(1 - \alpha\beta^{-1})(1 + \alpha) \quad (8)$$

This power can be supposed to be equal P_{DG} by neglecting the VSI losses. Therefore, the final expression demonstrating the relative active power variation $(\Delta P_{DIS})/P_{MPP}$ caused by the employed disturbance can be deduced as follows:

$$\begin{aligned} \frac{\Delta P_{DIS}}{P_{MPP}} &= ((1 - \alpha\beta^{-1})(1 + \alpha)) - 1 \\ &= -\alpha^2\beta^{-1} + \alpha(1 - \beta^{-1}) \end{aligned} \quad (9)$$

This equation can be solved for a given β and computed active power drop (-56.25%). For instance, the answers of (9) for PV module applied in the studied system with $\beta = 25\%$ are $+15.6\%$ (acceptable) and -90.5% (unacceptable). The validation of the computed setting is judged by simulating the system in the worst scenario ($V_{pr} = 110\%$ and $V_{po} = 88\%$) for $\alpha = 15$, 17.5 and 20%. The results in Fig. 16 clearly display that the 15% disturbance voltage cannot drive PCC voltage beyond 88%. Hence, the islanding cannot be efficiently recognized.

Therefore, $V_T = 0.4\%$ and $V_{DIS} = 0.2V_{MPP}$ are secure selections for method's thresholds providing $-0.805\% < \Delta P/P_{DG} < 0.795\%$ NDZ. These parameters are determined disregarding the system characteristics and can be easily developed for a given network.

V. Discussions

In the presented scheme, the DG output current has been declined significantly for the islanding detection purpose. This current drop may pose adverse effect on the performance of overcurrent relays (OCRs) and protection coordination. In this perspective, the effect of proposed IDM on OCRs performance has been initially investigated. A comparative analysis of the MPPT-based algorithm with a few existing IDMs is then carried out and presented as well.

A. Effect on Overcurrent Protection Relays

Distribution network is mainly protected against short-circuit faults by OCRs, including instantaneous, definite time (DT), and inverse time relays. In instantaneous OCR, the faulted area is de-energized without intentional time delay while this goal is fulfilled after a fixed and pre-decided time delay for a DT type. Equation (10) gives the operating time of the inverse time OCR, depending on short-circuit current level (I_F), i.e., higher current leads to a lower operating time (t_{op}) [34], [35]:

$$t_{op} = \frac{a \times TMS}{\left(\frac{I_F}{I_S}\right)^b - 1} \quad (10)$$

whereas *TMS* and I_S are the time multiplier setting and current setting, designed to coordinate primary and backup protections. This relay type can be further categorized into the normally inverse (NI), very inverse (VI), and extremely inverse (EI) subgroups regarding the level of a and b, e.g., $a = 80$ and $b = 2$ for EI type [35].

The effect of proposed MPPT-based algorithm on primary and backup OCRs of a radial distribution network during the fault event can be assessed by thaking into accunt the intentional 160 ms time delay needed for the disturbance activation, 300 ms time frame in which the disturbance is injected, and fault and OCR characteristics. According to the operating time of the OCR and fault characteristics, following scenarios can be observed:

- *Instantaneous and DT relays:* In these relays, the primary OCR actuates before disturbance injection regardless of the I_F level and it is not affected by the proposed algorithm (Fig. 17). For backup relay, the operating time (t_{op}^b) remains unchanged for $t_{op}^b \leq 160$ ms (red line in Fig. 17). In other states, the fault current seen by the backup OCR (I_F^b) drops notably regarding the method activation, may become lower than the current setting (I_S^b), and hence the relay would be reset. Therefore, the relay trips after disturbance clearance

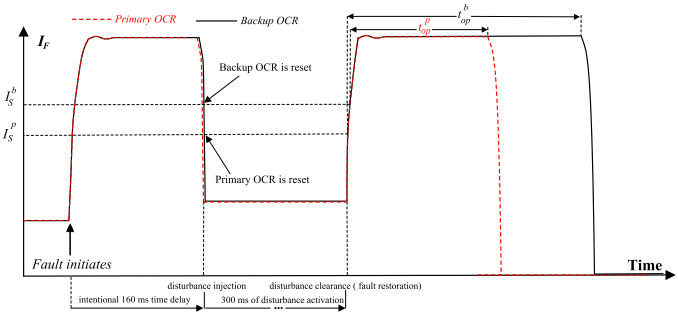

Fig. 18. Inverse time OCR performance at presence of presented IDM by supposing $t^p_{op} > 0.16$ s and $t^b_{op} > 0.16$ s.

and I_F restoration, and the operating time increases by 460 ms (green line in Fig. 17). This time delay includes the intentional 160 ms time delay as well as the 300 ms time frame in which the output current is dropped by the proposed technique. Besides, the protection coordination has not been deteriorated by the equipped algorithm in both states, i.e., backup does not trip before the main relay.

- *Inverse time relay under great short-circuit fault:* Inverse time primary OCR operates before disturbance injection under great I_Fs, i.e., $t^p_{op} \leq 160$ ms. These situations can be determined in terms of *TMS* using (10). For instance, a NI relay, with $a = 0.14, b = 0.02$, operates before 160 ms under I_F/I_S larger than 8.51 and 66.29 for 0.05 and 0.1 *TMS*, respectively. Since the backup inverse time relay should be activated at least 200 ms after primary OCR activation, t^b_{op} is raised by 460 ms through the employed disturbance; however, the protection system remains coordinated.
- *Inverse time relay under insignificant fault current:* If the main OCR has not been tripped by the sensed I_F before disturbance injection, the MPPT lost would raise relay operating time. In this condition, the reduced fault current may drop beyond I_S and OCR would be reset. The relay initiates again during the fault current restoration which occurs after removing the injected disturbance $(I_F \geq I_S)$ as shown in Fig. 18. Furthermore, the same current is seen by the backup OCR in radial network. The backup setting current is also chosen higher than the relay's current setting installed at downstream line regarding the greater load current in upstream network. Consequently, the same procedure is happened for backup relay, i.e., $I^b_S \geq I^p_S$, $I^p_F < I^p_S$, and $I^p_F = I^b_F$, then $I^b_F < I^b_S$. The backup OCR has been reset, and both relays observe the re-established fault current after removing the injected disturbance. The operating times of both OCRs are raised by 460 ms, and protection system remains coordinated (Fig. 18).

It can be concluded that the protection coordination of a radial network has not been affected by the recommended algorithm. Furthermore, the inverse time (primary and backup), instantaneous (backup), and DT (backup) relays' operating time may be raised by 460 ms through the injected disturbance. Luckily, this time interval does not pose a risk for connected loads during insignificant fault current [36]. The summary of method's influence on time delay of primary and backup OCRs (Δt^p_{op} and Δt^b_{op}) has been tabulated in Table VIII.

TABLE VIII
SUMMARY OF METHOD EFFECT ON OCRS IN RADIAL NETWORK

OCR type	Without proposed method		With proposed method	
	t^p_{op}	t^b_{op}	Δt^p_{op}	Δt^b_{op}
Simultaneous	≤0.16 s	≤0.16 s	–	–
and DT	≤0.16 s	>0.16 s	–	0.46 s
Inverse time	≤0.16 s	≤0.16 s	–	–
	≤0.16 s	>0.16 s	–	0.46 s
	>0.16 s	>0.16 s	0.46 s	0.46 s

B. Comparison With a Few Existing IDMs

It is concluded from the literature review that NDZ, detection time, capability to be implemented in microgrid, level of complexity and cost, and power quality degradation are paramount features considered for evaluation of the IDMs. A comparison between the proposed algorithm and recently IDMs developed to the GCPVS is provided as follows and summarized in Table IX.

- The performance of the computational-based algorithms in [18]–[20] depends highly on threshold(s). The threshold(s) determination also relies fully on the case study system features. Having said that, the settings of the proposed IDM can be easily determined regardless of the system characteristic.
- The VPF technique in [23], [24] suffers a wide NDZ for underloading cases concerning the inability to rise power generation and output voltage. The modification of VPF to fix this issue are reported in [25], [26]; however, these IDMs can only be employed for disconnecting DGs in traditional power system. Contrary to this, the current algorithm detects islanding with small NDZ and provides the chance to penetrate full power in standalone operation mode of microgrid by fast MPP restoration.
- The ratio of *d*–axis voltage to current components have been introduced for islanding classification of single GCPVS [27]. The equations under two DGs are complex and very hard for extension under multi DGs scenario, however. While the current MPPT injection-based IDM can be easily and inexpensively developed to multi DGs case.

VI. CONCLUSION

This paper proposes an accurate and fast IDM for GCPVSs applicable to microgrids. In the proposed scheme, a disturbance is triggered in the MPPT algorithm when the absolute output voltage deviation exceeds a threshold. Thereafter, this disturbance shifts the GCPVS operating point from MPP, resulting in a significant output power and voltage fall in islanded mode.

The provided HiL real-time simulations of the studied system equipped with two actual multi-functional digital relays underlined precise islanding detection under extensive scenarios defined by IEEE 1547-2008 and UL 1471 standards within 300 ms.

TABLE IX
COMPARISON OF THE PRESENTLY IDMS FOR GCPVS WITH CURRENT METHODOLOGY

Methodology	NDZ ($\Delta P/P_{DG}$)	Threshold dependency to the system settings	Detection Time (ms)	Applicable to microgrid?	Power quality degradation?	Complexity and cost
Modal current envelope [18]	Near zero	High	40–60	No	No	High
Forced Helmholtz oscillator [19]	-12 to 10%	High	Up to 1.13 s	Yes	No	High
VPF [23], [24]	0 to 17.355%	Medium	200–500	No	No	Low
Improved VPF [25], [26]	Near zero	Medium	200–300	No	No	Low
d–axis resistance [27]	Zero	High	Up to 800	No	Yes	High
Proposed algorithm	**Near zero**	**Low**	**200–300**	**Yes**	**No**	**Low**

The NDZ includes a narrow $-0.805\% < \Delta P/P_{DG} < 0.795\%$ bound and the method provides the chance of power restoration at MPP for autonomous operation of microgrid. The outputs of the non-islanding events such as motor starting, capacitor switching, and sudden load variation also reveal that although P_{DG} drop is inevitable for a short duration; the voltage remains in the permissible limits due to the network presence. Additionally, an intentional time delay is designed for method activation after short-circuit fault clearance, leading to UV-ride through capability. This 0.16 s time delay may increase the OCR clearing time under insignificant short-circuit fault current which does not pose a risk to the local demands. Nevertheless, a further study is mandatory for a substation backup protection with 600–700 ms operating time to ensure its precise protection.

The explicit terms have been deduced to determine the thresholds regardless of the system settings and DG's penetration level. Moreover, it has been shown that the implementation of the proposed algorithm is cost-competitive and simple. Therefore, it is a well-defined IDM for GCPVSs according to the overall aforementioned superiorities.

REFERENCES

[1] "2019 snapshot of global PV markets," International Energy Agency, Paris, France, Report IEA PVPS T1-35: 2019.

[2] C. Li, C. Cao, Y. Cao, Y. Kuang, L. Zeng, and B. Fang, "A review of islanding detection methods for microgrid," *Renewable Sustain. Energy Rev.*, vol. 35, pp. 211–220, Jul. 2014.

[3] *IEEE Standard for Interconnecting Distributed Resources with Electric Power Systems*, IEEE Standard 1547–2008, 2008.

[4] *Standard for Inverters, Converters, Controllers and Interconnection System Equipment for Use With Distributed Energy Resources*, UL 1741, Jan. 2010.

[5] T. John and S. P. Lam, "Voltage and frequency control during microgrid islanding in a multi-area multi-microgrid system," *IET Gener., Transmiss. Distribution*, vol. 11, no. 6, pp. 1502–1512, Apr. 2017.

[6] W. Wang, J. Kilber, and W. Xu, "A scalable power line signaling based scheme for islanding detection of distributed generators," *IEEE Trans. Power Del.*, vol. 24, no. 2, pp. 903–909, Apr. 2009.

[7] G. Bayrak and E. Kabalci, "Implementation of a new remote islanding detection method for wind–solar hybrid power plants," *Renewable Sustain. Energy Rev.*, vol. 58, pp. 1–15, May 2016.

[8] J. C. M. Vieira, W. Freitas, W. Xu, and A. Morelato, "Performance of frequency relays for distributed generation protection," *IEEE Trans. Power Del.*, vol. 21, no. 3, pp. 1120–1127, Jul. 2006.

[9] J. C. M. Vieira, D. S. Correa, W. Freitas, and W. Xu, "Performance curves of voltage relays for islanding detection of distributed generators," *IEEE Trans. Power Syst.*, vol. 20, no. 3, pp. 1660–1662, Aug. 2005.

[10] C. M. Affonso, W. Freitas, W. Xu, and L. C. P. Da Silva, "Performance of ROCOF relays for embedded generation applications," *IEE Proc. Gener., Transmiss. Distribution*, vol. 152, no. 1, pp. 109–114, Jan. 2005.

[11] R. Bekhradian, M. Davarpanah, and M. Sanaye-Pasand, "Novel approach for secure islanding detection in synchronous generator based microgrids," *IEEE Trans. Power Del.*, vol. 34, no. 2, pp. 457–466, Apr. 2019.

[12] S. Nikolovski, H. R. Baghaee, and D. Mlakic, "Islanding detection of synchronous generator-based DGs using rate of change of reactive power," *IEEE Syst. J.*, vol. 13, no. 4, pp. 4344–4354, Dec. 2019.

[13] A. G. Abd-Elkader, S. M. Saleh, and M. B. Magdi Eiteba, "A passive islanding detection strategy for multi-distributed generations," *Int. J. Elect. Power Energy Syst.*, vol. 99, pp. 146–155, Jul. 2018.

[14] B. Guha, R. J. Haddad, and Y. Kalaani, "Voltage ripple-based passive islanding detection technique for grid-connected photovoltaic inverters," *IEEE Power Energy Technol. Syst. J.*, vol. 3, no. 4, pp. 143–154, Dec. 2016.

[15] Q. Cui, K. El-Arroudi, and G. Joos, "Islanding detection of hybrid distributed generation under reduced non-detection zone," *IEEE Trans. Smart Grid*, vol. 9, no. 5, pp. 5027–5037, Sep. 2018.

[16] D. Mlakic, H. R. Baghaee, and S. Nikolovski, "A novel ANFIS-based islanding detection for inverter-interfaced microgrids," *IEEE Trans. Smart Grid*, vol. 10, no. 4, pp. 4411–4424, Jul. 2019.

[17] H. T. Do, X. Zhang, N. V. Nguyen, S. Li, and T. T.-T. Chu, "Passive islanding detection method using wavelet packet transform in grid connected photovoltaic systems," *IEEE Trans. Power Electron.*, vol. 31, no. 10, pp. 6955–6967, Oct. 2016.

[18] R. Haider *et al.*, "Passive islanding detection scheme based on autocorrelation function of modal current envelope for photovoltaic units," *IET Gener., Transmiss. Distribution*, vol. 12, no. 3, pp. 726–736, Feb. 2018.

[19] M. Bakhshi, R. Noroozian, and G. B. Gharehpetian, "Novel islanding detection method for multiple DGs based on forced Helmholtz oscillator," *IEEE Trans. Smart Grid*, vol. 9, no. 6, pp. 6448–6460, Nov. 2018.

[20] P. P. Mishra and C. N. Bhende, "Islanding detection using sparse S-transform in distributed generation systems," *Elect. Eng.*, vol. 100, no. 4, pp. 2397–2406, Jul. 2018.

[21] H. F. Xiao, Zh. Fang, D. Xu, B. Venkatesh, and B. Singh, "Anti–islanding protection relay for medium voltage feeder with multiple distributed generators," *IEEE Trans. Ind. Electron.*, vol. 64, no. 10, pp. 7874–7885, Oct. 2017.

[22] P. Gupta, R. S. Bhatia, and D. K. Jain, "Active ROCOF relay for islanding detection," *IEEE Trans. Power Del.*, vol. 32, no. 1, pp. 420–429, Feb. 2017.

[23] F. Lin, Y. Huang, K. Tan, J. Chiu, and Y. Chang, "Active islanding detection method using *d*–axis disturbance signal injection with intelligent control," *IET Gener., Transmiss. Distribution*, vol. 7, no. 5, pp. 537–550, May 2013.

[24] A. Samui and S. R. Samantaray, "An active islanding detection scheme for inverter–based DG with frequency dependent ZIP–Exponential static load mode," *Int. J. Elect. Power Energy Syst.*, vol. 78, pp. 41–50, Jun. 2016.

[25] R. Bakhshi and J. Sadeh, "Voltage positive feedback based active method for islanding detection of photovoltaic system with string inverter using sliding mode controller," *Solar Energy*, vol. 137, pp. 564–577, Nov. 2016.

[26] S. Liu, S. Zhuang, Q. Xu, and J. Xiao, "Improved voltage shift islanding detection method for multi-inverter grid-connected photovoltaic systems," *IET Gener., Transmiss. Distribution*, vol. 10, no. 13, pp. 3163–3169, Oct. 2016.

[27] D. Sivadas and K. Vasudevan, "An active islanding detection strategy with zero non-detection zone for operation in single and multiple inverter mode using GPS synchronized pattern," *IEEE Trans. Ind. Electron.*, to be published, doi: 10.1109/TIE.2019.2931231.

[28] X. Chen, Y. Li, and P. Crossley, "A novel hybrid islanding detection method for grid-connected microgrids with multiple inverter-based distributed generators based on adaptive reactive power disturbance and passive criteria," *IEEE Trans. Power Electron.*, vol. 34, no. 9, pp. 9342–9356, Sep. 2019.

[29] A. Rostami, A. Jalilian, S. Zabihi, J. Olamaei, and E. Pouresmaeil, "Islanding detection of distributed generation based on parallel inductive impedance switching," *IEEE Syst. J.*, vol. 14, no. 1, pp. 813–823, Mar. 2020.

[30] H. Athari, M. Niroomand, and M. Ataei, "Review and classification of control systems in grid–tied inverters," *Renewable Sustain. Energy Rev.*, vol. 72, pp. 1167–1176, May 2017.
[31] R. Ahmad, A. F. Murtaza, and H. A. Sher, "Power tracking techniques for efficient operation of photovoltaic array in solar applications– A review," *Renewable Sustain. Energy Rev.*, vol. 101, pp. 82–102, Mar. 2019.
[32] *IEEE Recommended Practice for Utility Interface of Photovoltaic (PV) Systems*, IEEE Standard 929–2000, 2000.
[33] O. W. Yin and B. C. Babu, "Simple and easy approach for mathematical analysis of photovoltaic (PV) module under normal and partial shading conditions," *Optik*, vol. 169, pp. 48–61, Sep. 2018.
[34] A. Sharma, D. Kiran, and B. K. Panigrahi, "Planning the coordination of overcurrent relays for distribution systems considering network reconfiguration and load restoration," *IET Gener., Transmiss. Distribution*, vol. 12, no. 7, pp. 1672–1679, Mar. 2018.
[35] P. N. Korde and P. P. Bedekar, "Optimal overcurrent relay coordination in distribution system using nonlinear programming method," in *Proc. 2016 Int. Conf. Elect. Power Energy Syst.*, Dec. 2016.
[36] A. Honrubia-Escribano, E. Gómez-Lázaro, A. Molina-García, and J. A. Fuentes, "Influence of voltage dips on industrial equipment: Analysis and assessment," *Int. J. Elect. Power Energy Syst.*, vol. 41, no. 1, pp. 87–95, Oct. 2012.

Reza Bakhshi-Jafarabadi was born in Mashhad, Iran, in 1988. He received the B.Sc. and M.Sc. degrees in electrical engineering from the Ferdowsi University of Mashhad, Mashhad, Iran, in 2011 and 2014, respectively. He is currently working toward the Ph.D. degree with the Department of Electrical Engineering, Ferdowsi University of Mashhad. His research interests include renewable energy technologies and integration of distributed generators into the power system.

Javad Sadeh was born in Mashhad, Iran, in 1968. He received the B.Sc. and M.Sc. degrees in electrical engineering (Hons.) from the Ferdowsi University of Mashhad, Mashhad, Iran, in 1990 and 1994, respectively, and the Ph.D. degree in electrical engineering from the Sharif University of Technology, Tehran, Iran, with the collaboration of the electrical engineering laboratory of the Institut National Polytechnique de Grenoble, Grenoble, France, in 2001. He is currently a Professor with the Department of Electrical Engineering, Ferdowsi University of Mashhad. He is also Educational Office Manager with the Ferdowsi University of Mashhad. His research interests are power system protection, dynamics, operation as well as renewable energy technologies.

Marjan Popov (Senior Member, IEEE) received the Dipl-Ing. degree in electrical power engineering from the University of Saints Cyril and Methodius of Skopje, Skopje, North Macedonia, in 1993, and the Ph.D. degree in electrical power engineering from the Delft University of Technology, Delft, The Netherlands, in 2002.

He is a Chevening Alumnus and in 1997, he was an Academic Visitor with the University of Liverpool, Liverpool, U.K., working in the Arc Research Group on modeling SF6 circuit breakers. His major research interests include future power systems, large-scale power system transients, intelligent protection for future power systems, and wide-area monitoring and protection. He is a member of CIGRE and actively participated in WG C4.502 and WG A2/C4.39. In 2010, he was the recipient of the prestigious Dutch Hidde Nijland Prize for extraordinary research achievements. He is the recipient of IEEE PES Prize Paper Award and IEEE Switchgear Committee Award for 2011. He is an Associate Editor for the Elsevier's *International Journal of Electric Power and Energy Systems*.